Effects of the γ-soft isomeric states on the giant monopole resonances in even-even cadmium isotopes ^{110,112,114,116}Cd

Xuwei Sun⊙, Jing Chen, and Dinghui Lu

Department of Physics, Zhejiang University, 310027 Hangzhou, China

The shape evolutions of the even-even cadmium isotopes $^{110-116}$Cd are investigated in this work. The giant monopole resonances built on different shape isomeric states are studied using the quasiparticle random phase approximation, which is implemented with a finite amplitude method. We find the local minima corresponding to the prolate, oblate, and triaxial-deformed isomeric states in the even-even cadmium isotopes. Their responses to external monopole perturbations are quite different. Larger deformation tends to make the energy of the giant monopole resonance to shift lower. It is well known that the density functional models have some difficulties in predicting the right positions of the monopole resonances in cadmium isotopes: the centroid energies always seem too large compared to the experimental results. Our calculations show the giant monopole resonances built on the γ soft isomeric states in the cadmium isotopes have centroid energies even lower than the experimental measurements. Therefore, if the isomeric branching of these γ soft isomeric states turns out to be prominent, isomer mixing may be a good explanation to the longstanding puzzle.

I. INTRODUCTION

For the infinite nuclear matter, the incompressibility K_∞ measures the stiffness of the equation of state (EoS), whose empirical value is roughly 240 ± 20 MeV. It can be extrapolated by analyzing the finite nucleus modulus K_A [1]. The latter is closely related to the centroid energy of the giant monopole resonance (GMR), or the breathing mode: $E_c \propto \sqrt{K_A}$ [2]. Nowadays, models based on the self-consistent mean field (SCMF) theory [3], or the nuclear density functional theory (DFT) [4] are able to predict the GMR of a lot of nuclei, such as ^{90}Zr and ^{208}Pb, with desirable precisions. However, they always meet serious challenges in tin or cadmium isotopes [2,5–7]. The experimental results are significantly lower that the theoretical predictions. Attempts were made to understand the theoretical overestimations, such as focusing on the role of the pairing interaction [8]. It is also interesting to check whether nuclear structure effect will have an impact.

Like many other nuclear phenomena, the evolution of an atomic nuclei's shapes manifests a clear shell effect: a nucleus tends to be spherical near the closed shells, and changes to more deformed shape towards the open shells. This kind of deformation is determined by the neutron/proton numbers, and the evolutions of the excitation properties will be affected by the deformation, such as stagnating the pygmy dipole resonance [9] and splitting the monopole resonance [10,11]. On the other hand, for some nuclei there is a more interesting feature that metastable states relating to particular deformations may emerge. The shape isomeric state, or the so-called shape isomer [12], is at the local minima of the potential energy surface (PES), which usually appears as a low-lying 0^+ state [13–15]. Shape isomerism has been reported in several research papers [16,17] and recently it is under intense discussions [18–22]. They differ from the ground state not only in energies and geometries, but also in physical configurations,

such as neutron/proton single particle levels, occupations of each orbital, etc.; hence influence the excitation properties in distinct ways. For example, the pygmy dipole resonance built on the prolate shape isomeric state in ^{68}Ni is about 1.5 MeV higher than that on the ground spherical state [23].

Random phase approximation (RPA), or quasiparticle random phase approximation (QRPA), treats the excitations of a nuclear system as the coherent transitions between different particle-hole or two-quasiparticle configurations [24], and is particularly efficient to describe the small amplitude oscillations around an equilibrium position. Therefore it is widely used in the studies of nuclear low-lying vibrations [25–28]. However, for axial and triaxial deformed systems, the configuration space of (Q)RPA problem becomes huge and the diagonalization of the (Q)RPA equation is critically time-consuming. One applicable approach to solve a large scale (Q)RPA problem is the finite amplitude method (FAM), which was first proposed by Nakatsukasa *et al.* [29]. The computation resource costs (CPU times and memories) of FAM increase almost linearly with the dimension of the configuration space. Therefore, it shows dramatic advantages over the conventional (Q)RPA scheme and becomes more and more popular in recent years [30–32].

In this work, we will establish the FAM scheme under the triaxial deformed condition, based on a covariant density functional model. Then we will investigate the impact of the shape isomeric state on the nuclear low-lying breathing mode.

II. SOLVING QRPA PROBLEM WITH THE FINITE AMPLITUDE METHOD

A. General frameworks of the finite amplitude method

The state of a nuclear system $|\psi\rangle$ can be determined uniquely by the single particle operator $\hat{\rho}$. It is improved by

Valatin *et al.* [33] to the generalized density $\hat{\mathcal{R}}$, in order to deal with the pairing correlations in superfluid systems. In the space expanded by a set of single particle basis $(c, c^{\dagger})$, for example the harmonic oscillator (H.O.) basis, the super matrix of the generalized density operator is

$$\hat{\mathcal{R}} = \begin{pmatrix} \rho & \kappa \\ -\kappa^* & 1 - \rho^* \end{pmatrix}, \qquad (1)$$

where κ is the pairing tensor, whose matrix elements in the particle basis are defined by $\kappa_{ij} \equiv \langle c_j c_i \rangle$. The energy of the nuclear system ϵ can be expressed as a functional of $\hat{\mathcal{R}}$, or equivalently, of $\hat{\rho}$ and $\hat{\kappa}$. The quasiparticle Hamiltonian is derived from the variation of the energy density functional, with respect to the generalized density operator,

$$\hat{\mathcal{H}} = \frac{\delta \epsilon[\hat{\mathcal{R}}]}{\delta \hat{\mathcal{R}}} = \begin{pmatrix} h & \Delta \\ -\Delta^* & -h^* \end{pmatrix}. \qquad (2)$$

The diagonalization of the generalized quasiparticle Hamiltonian $\hat{\mathcal{H}}$ leads to the so-called Hartree-Bogoliubov equation:

$$\mathcal{W} \begin{pmatrix} h - \lambda & \Delta \\ -\Delta^* & -h^* + \lambda \end{pmatrix} \mathcal{W}^{\dagger} = \begin{pmatrix} E & 0 \\ 0 & -E \end{pmatrix}, \qquad (3)$$

where λ is the chemical potential accounting for the particle number conservation [24]. From Eq. (3) one can get the quasiparticle spectrum E as well as the transformation matrix

$$\mathcal{W} = \begin{pmatrix} U & V^* \\ V & U^* \end{pmatrix}. \qquad (4)$$

The transformation between the single particle space and the quasiparticle space is unitary and defines the quasiparticle creation and annihilation operators as

$$\begin{pmatrix} \beta \\ \beta^{\dagger} \end{pmatrix} = \mathcal{W}^{\dagger} \begin{pmatrix} c \\ c^{\dagger} \end{pmatrix}. \qquad (5)$$

Generally, a single particle operator $\hat{O}$ can be expressed in the quasiparticle space as

$$\hat{O} = \frac{1}{2} \sum_{\mu\nu} \left\{ O^{20}_{\mu\nu} \boldsymbol{A}^{\dagger}_{\mu\nu} + O^{02}_{\mu\nu} \boldsymbol{A}_{\mu\nu} + O^{11}_{\mu\nu} \boldsymbol{B}_{\mu\nu} + \text{H.c.} \right\}, \qquad (6)$$

where $\boldsymbol{A}_{\mu\nu} = \hat{\beta}^{\dagger}_{\mu} \hat{\beta}^{\dagger}_{\nu}$ and $\boldsymbol{B}_{\mu\nu} = \hat{\beta}^{\dagger}_{\mu} \hat{\beta}_{\nu}$ are two quasiparticle operators. The matrix elements of a one-body variable $\hat{O}$ can be easily transformed from the quasiparticle basis to the harmonic oscillator basis as

$$\hat{O}_{\text{H.O.}} = \mathcal{W} \hat{O}_{qp} \mathcal{W}^{\dagger}, \qquad (7)$$

and vice versa.

When the nuclear system is perturbed by an external field

$$\mathcal{F}(t) = F e^{-i\omega t} + \text{H.c.}, \qquad (8)$$

the generalized density operator $\mathcal{R}$ changes according to the time dependent relativistic Hartree-Bogoliubov (TDRHB) equation [11]

$$i\dot{\mathcal{R}}(t) = [\mathcal{H}(t) + \mathcal{F}(t), \mathcal{R}(t)]. \qquad (9)$$

As long as the external perturbation is weak, it only drives the density operator and Hamiltonian to oscillate

harmonically,

$$\mathcal{R}(t) = \mathcal{R}_0 + \delta R(\omega) e^{-i\omega t} + \text{H.c.},$$
$$\mathcal{H}(t) = \mathcal{H}_0 + \delta H(\omega) e^{-i\omega t} + \text{H.c.} \qquad (10)$$

The generalized density $\mathcal{R}$ is a projection operator, which means $\mathcal{R}^2 = \mathcal{R}$. Therefore, in the quasiparticle space where $\mathcal{H}_0$ and $\mathcal{R}_0$ are diagonalized, the variation of the generalized density reads

$$\delta R(\omega) = \sum_{\mu\nu} \{ X_{\mu\nu}(\omega) \boldsymbol{A}^{\dagger}_{\mu\nu} + Y_{\mu\nu}(\omega) \boldsymbol{A}_{\mu\nu} \}, \qquad (11)$$

while the terms relating to $\boldsymbol{B}_{\mu\nu}$ and its conjugation vanish. To be specific, according to Eq. (7), the transition density δR transforms as

$$\begin{pmatrix} \delta\rho & \delta\kappa \\ -\delta\kappa^* & -\delta\rho^* \end{pmatrix} = \mathcal{W} \begin{pmatrix} 0 & X \\ Y & 0 \end{pmatrix} \mathcal{W}^{\dagger}. \qquad (12)$$

Meanwhile, the variation of Hamiltonian δH transforms as

$$\begin{pmatrix} \delta H^{11} & \delta H^{20} \\ -\delta H^{02} & -\delta H^{11*} \end{pmatrix} = \mathcal{W}^{\dagger} \begin{pmatrix} \delta h & \delta\Delta \\ -\delta\Delta^* & -\delta h^* \end{pmatrix} \mathcal{W}. \qquad (13)$$

Inserting the above equations into Eq. (9), we can get the linear response equation:

$$(E_{\mu} + E_{\nu} - \omega) X_{\mu\nu}(\omega) + \delta H^{20}_{\mu\nu}(\omega) = -F^{20}_{\mu\nu},$$
$$(E_{\mu} + E_{\nu} + \omega) Y_{\mu\nu}(\omega) + \delta H^{02}_{\mu\nu}(\omega) = -F^{02}_{\mu\nu}. \qquad (14)$$

The linear response equation takes a simple form in the quasiparticle space, while the variation of Hamiltonian and pairing potential are more convenient to calculate in the oscillator basis. In the spirit of FAM, the variation of the single particle Hamiltonian is calculated via the numerical differentiation,

$$\delta h = \frac{1}{\eta} (h[\rho_0 + \eta\delta\rho] - h[\rho_0]), \qquad (15)$$

so are the variations of the pairing potential

$$\delta\Delta = \frac{1}{\eta} (\Delta[\kappa_0 + \eta\delta\kappa] - \Delta[\kappa_0]),$$
$$\delta\Delta^* = \frac{1}{\eta} (\Delta^*[\kappa_0^* + \eta\delta\kappa^*] - \Delta^*[\kappa_0^*]). \qquad (16)$$

η is a small real number introduced to induce a numerical difference [11,29], which is independent to the physical results. A major convenience of FAM is that one can take advantages of the procedures $h[\hat{\rho}]$ and $\Delta[\hat{\kappa}]$ of the ground state DFT solver when calculating the corresponding numerical variations. For instance, in this work the calculation is performed based on the relativistic self-consistent mean-field program package DIRHB [34].

For a given ω, the FAM starts with an initial guess of X^0, Y^0 (e.g., 0 or the results from an adjacent ω), the iterations proceed as follows: (i) use Eq. (12) to get the transition densities $\delta\rho$, $\delta\kappa$, and $\delta\kappa^*$ from X^i and Y^i; (ii) calculate the variations of the single particle Hamiltonian δh through Eq. (15) and the pairing potentials $\delta\Delta$, $\delta\Delta^*$ through Eq. (16); (iii) transform to quasiparticle space as Eq. (13) to get δH^{02} and δH^{20}; (iv) update the transition density X^{i+1} and Y^{i+1} according to

Eq. (14); (v) repeat steps (i) to (iv) with the updated X and Y until the series $X^0, X^1, X^2, \ldots, X^n$ and $Y^0, Y^1, Y^2, \ldots, Y^n$ converge.

The strength function then can be obtained from the forward and backward transition densities X and Y, which reads

$$\frac{dB(F;\omega)}{d\omega} = -\frac{1}{\pi}\text{Im}\sum_{\mu\nu}\left\{F_{\mu\nu}^{20*}X_{\mu\nu}(\omega) + F_{\mu\nu}^{02*}Y_{\mu\nu}(\omega)\right\}. \quad (17)$$

B. Covariant nuclear density functional model with density-dependent meson-nucleon couplings

In the following, we will introduce the density functional that is used in our calculation briefly. In this work, the density functional ϵ^{ph} accounting for the long range correlations between nucleons is constructed with the relativistic density-dependent meson-exchange model. The parameter set used is DD-ME2 [35]. The interactions between nucleons are described by the following Lagrangian:

$$\mathcal{L}_{\text{int}} = -g_\sigma \bar{\psi}\psi\sigma - g_\omega \bar{\psi}\gamma^\mu\psi\omega_\mu$$
$$- g_\rho \bar{\psi}\vec{\tau}\gamma^\mu\psi \cdot \vec{\rho}_\mu - e\bar{\psi}\gamma^\mu\frac{1-\tau_3}{2}\psi A_\mu. \quad (18)$$

The effective nuclear forces are transmitted by the σ, ω, $\vec{\rho}_\mu$ mesons and the photon, with the corresponding coupling strengths $g_i(\rho)(i = \sigma, \omega, \rho)$ and e. The Hamiltonian density is a component of the energy-momentum tensor,

$$\mathcal{H} = T^{00} = \frac{\partial\mathcal{L}}{\partial\dot{q}_i}\dot{q}_i - \mathcal{L}, \quad (19)$$

where q_i represents the nucleon, mesons, and electromagnetic fields. The equations of motion of mesons can be obtained from Euler-Lagrangian equation, which turns out to be

$$\left(\partial^\nu\partial_\nu + m_\sigma^2\right)\sigma = -g_\sigma\bar{\psi}\psi,$$
$$\left(\partial^\nu\partial_\nu + m_\omega^2\right)\omega^\mu = g_\omega\bar{\psi}\gamma^\mu\psi,$$
$$\left(\partial^\nu\partial_\nu + m_\rho^2\right)\vec{\rho}^\mu = g_\rho\bar{\psi}\vec{\tau}\gamma^\mu\psi,$$
$$\partial^\nu\partial_\nu A^\mu = e\bar{\psi}\gamma^\mu\frac{1-\tau_3}{2}\psi. \quad (20)$$

Taking the expectation values of Eq. (20) leads to

$$\left(-\Delta + m_m^2\right)\phi_m = \mp g_m\rho_m, \quad (21)$$

where $m = \sigma, \omega, \rho, A$; m_m denotes meson mass m_σ, m_ω, m_ρ, and equals zero for the photon. ϕ_m represents the expectation value of each meson field or electromagnetic field. The densities ρ_m are

$$\rho_s = \langle\bar{\psi}\psi\rangle, \quad \rho_v = \langle\bar{\psi}\gamma^0\psi\rangle,$$
$$\rho_{vt} = \langle\bar{\psi}\tau_3\gamma^0\psi\rangle, \quad \rho_c = \left\langle\bar{\psi}\gamma^0\frac{1-\tau_3}{2}\psi\right\rangle. \quad (22)$$

In the no-sea approximation [36] which means omitting antiparticle terms in the nucleon field, Eq. (22) can be expressed as functionals of the density operator

$$\rho_s = \text{Tr}[\gamma^0\rho], \quad \rho_v = \text{Tr}[\rho],$$
$$\rho_{vt} = \text{Tr}[\tau_3\rho], \quad \rho_c = \text{Tr}\left[\frac{1-\tau_3}{2}\rho\right]. \quad (23)$$

Then the meson fields and the electromagnetic field can be solved from Eq. (21), and can be eliminated from the energy density functional

$$\epsilon^{ph}[\rho, \phi] = \left\langle\int\mathcal{H}d^3\mathbf{r}\right\rangle$$
$$= \text{Tr}[(-i\boldsymbol{\alpha}\nabla + \beta m)\rho] + \frac{1}{2}\int d^3r g_m\phi_m\rho_m. \quad (24)$$

The single particle Hamiltonian is derived by variation of the energy density functional with respect to the single particle density

$$\hat{h} = \frac{\delta\epsilon^{ph}}{\delta\rho} = -i\boldsymbol{\alpha}\nabla + \beta M^* + V, \quad (25)$$

where the effective nucleon mass and the vector potential are

$$M^* = m + g_\sigma\sigma,$$
$$V = g_\omega\omega + g_\rho\tau_3\rho + \frac{1-\tau_3}{2}A + \Sigma_0^R. \quad (26)$$

The last term Σ_0^R in the vector potential is the rearrangement term [34], which comes from the density dependence of the coupling constants. The paring potential is a functional of the pairing tensor

$$\hat{\Delta} = \tfrac{1}{2}\text{Tr}[V^{pp}\kappa]. \quad (27)$$

The pairing interaction V^{pp} is treated with a finite range separable force [37]

$$V^{pp}(\mathbf{r}_1, \mathbf{r}_2, \mathbf{r}_1', \mathbf{r}_2') = -G\delta(\mathbf{R} - \mathbf{R}')P(\mathbf{r})P(\mathbf{r}'). \quad (28)$$

C. Validation of the numerical implementation

In conventional (Q)RPA calculations which diagonalize the (Q)RPA equation directly [9,38], the strength function is usually calculated by folding the transition probability B_ν of each state ω_ν:

$$\frac{dB(F,\omega)}{d\omega} = \frac{1}{\pi}\sum_\nu B_\nu\frac{\Gamma/2}{(\omega - \omega_\nu)^2 + (\Gamma/2)^2}. \quad (29)$$

In finite amplitude method no eigenstates are actually calculated. To avoid the singularity of Eq. (14) when calculating X and Y in the vicinity of $\omega = E_\mu + E_\nu$, an imaginary factor $i\gamma$ is added into ω. This is equivalent to smear the strength distribution with a Lorentz function as Eq. (29), with a width $\Gamma = 2\gamma$ [11,39]. The parameter η which induces a numerical difference is chosen as 10^{-6}, and will be used here and in all the following calculations. The Broyden mixing method [40] is used to accelerate the iteration procedures. The iteration stops when the relative residual of two sequential vectors (X, Y) is less than 10^{-8}, which typically requires about 50 iterations. However, at some ω near the peaks, several hundreds of iterations may be needed.

When a nuclear system is solved within RHB models, the particle number conservation, which is a symmetry of the Hamiltonian, is broken. Therefore, a zero energy Goldstone boson is generated as a result of the spontaneous symmetry breaking. The spurious state corresponding to the particle number operator $\hat{N}$ will be obtained by fully self-consistent
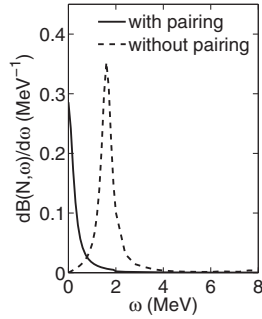
FIG. 1. Validation of the numerical implementation in the example nucleus ^{20}Ne: Decoupling of the spurious state. The strength in the no pairing case is divided by 10.

FAM calculations. Actually, the decoupling of the spurious state is a stringent test for the numerical implementation, which requires a self-consistent treatment of both the ground state and the excitation state. In covariant density functional calculations, it is essential to include the anti-particle states as well [25]. Benefiting from the efficiency of the FAM scheme, the whole configuration involving the antiparticle states can be easily taken into account. Indeed, except for N_F (number of oscillator shells [34], which controls the dimension of the basis space, is set to 20 in our FAM calculations, that makes the most results converge), no further truncations on the two-quasiparticle configuration space are introduced in our self-consistent calculations.

To validate the numerical implementation, we use the nucleus ^{20}Ne as an example. The strength function of the particle number operator $\hat{N}$ are calculated with a spacing 0.1 MeV, as illustrated with the solid and dashed lines in Fig. 1. When the pairing interaction is omitted in the FAM calculation (yet still included in the RHB calculation), the peak of the strength function locates at about 1.6 MeV. In contrast, if the pairing interaction is properly treated, the self-consistency will be fulfilled. We find that the calculation data can be well fitted by the following function [with a residual sum of squares (RSS) about 5.27×10^{-6}]:

$$f(\omega) = \frac{0.01834}{(\omega + 0.0624)^2 + 0.2499^2}, \qquad (30)$$

which describes a Lorentzian function centering at $\omega_0 = -0.0624$ MeV and with a width $\Gamma = 0.499$ MeV. This means the strength of the particle number operator is almost exhausted by the single state locating at the nearly vanishing energy, i.e., the spurious state. Therefore, the particle-number-rotation symmetry broken by the RHB treatment is restored by the FAM calculation. As the spurious state has been well separated, the other physical excitation states will not be contaminated. This is crucial to get the correct results in the giant resonance area.

III. RESULTS AND DISCUSSIONS

A. Shape isomeric states in even-even Cd isotopes

In spherical nuclei, the single particle levels belonging to the same angular momentum j are degenerate. When the
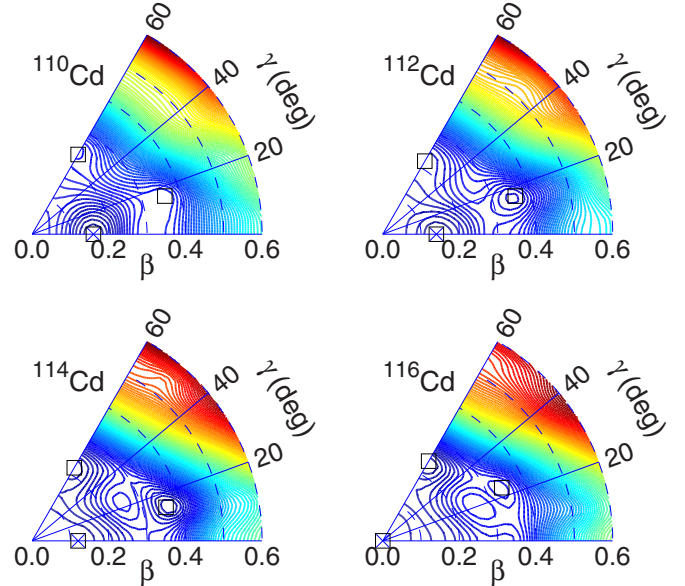

FIG. 2. Potential energy surfaces of the Cd isotopes, the contours are drawn with spacings of 0.2 MeV. In the PESs, the squares □ represent the local minima and the crosses × represent the ground states.

nuclei are deformed, they will split into $(2j + 1)/2$ orbitals, retaining twofold degeneracy as a result of Kramers' theorem [41]. The deformation affects the way the single particle levels split, as well as the occupation of each orbital. As a result, the physical observable of a nucleus, such as the energy, will change accordingly. The mean-field state is the lowest order approximation to the eigenstate of the total many-body Hamiltonian. Based on it, we calculated the potential energy surface (PES), which is a function of the deformation parameters. The deformation of a nucleus can be described by the Hill-Wheeler coordinates β and γ [24,42], which are used in the DFT solver DIRHB [34]. In the case of $\gamma = 0$, it describes a prolate shape which is like a lemon; in the case of $\gamma = 60$, it describes an oblate shape which is like an orange. The other value of γ describes a triaxial deformed shape, or a γ soft shape, whose any intersecting line perpendicular to its reflection axis is an ellipse. In our work, the energy of a nucleus is calculated in a finite-size grid (31×31 points), i.e., β from 0 to 0.6 with a spacing of 0.02 and γ from $0°$ to $60°$ with a spacing of $2°$. The results are drawn in Fig. 2 with contours spaced by 0.2 MeV, in which the ground states and all the isomeric states are also indicated by the cross and square markers. Except for the nucleus ^{116}Cd which is spherical, other cadmium isotopes are all prolate in their ground states. As we can learn from the PESs, when the nucleus is stretched to a prolate shape with β larger than 0.4, or is squeezed to an oblate shape with β larger than 0.3, the energy will increase rapidly and monotonously. In the area where a physical deformation is possible, several local minima exist in all the Cd isotopes, which we call the shape isomeric states. Some of them are prolate, some are oblate, and in each Cd isotope there is a γ-soft state. The presence

TABLE I. Local minima of the PESs in the Cd isotopes, calculated using the relativistic density functional DD-ME2. In the second column is the first local minimum of each nucleus, i.e., the ground state (g.s.). The energy of each local minima with respect to g.s. (in MeV) is listed after its deformation coordinates (β, γ).

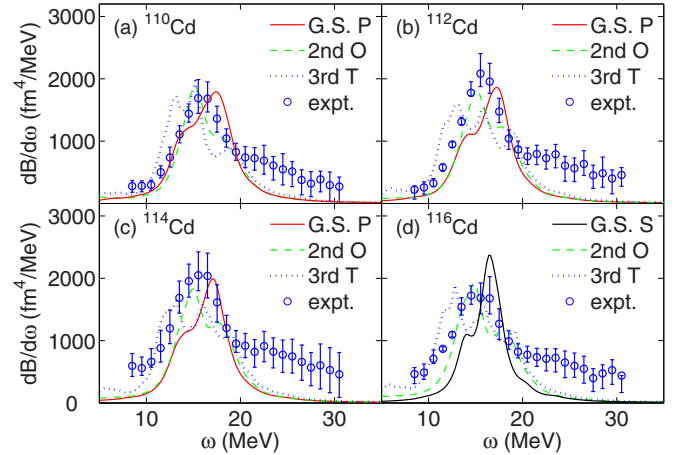| Nucl.	g.s.	2nd		3rd	
^{110}Cd	$(0.16, 0°)$	$(0.24, 60°)$	2.37	$(0.36, 16°)$	2.60
^{112}Cd	$(0.14, 0°)$	$(0.22, 60°)$	1.06	$(0.36, 16°)$	1.12
^{114}Cd	$(0.12, 0°)$	$(0.22, 60°)$	0.06	$(0.36, 14°)$	0.40
^{116}Cd	$(\beta = 0)$	$(0.24, 60°)$	0.007	$(0.34, 24°)$	1.44

FIG. 3. The strength functions of GMR in the Cd isotopes. The solid lines represent the strength functions corresponding to the ground states, and dashed lines, dotted lines represent the results built on the second, and third isomeric states, respectively. The shapes of each isomeric state are also represented: S for spherical, P for prolate, O for oblate, and T for triaxial-deformed.

of the shape isomers in Cd isotopes is also predicted by the previous theoretical investigation [19].

Although the appearances of the local minima in the Cd isotopes show some similarities, there are also prominent differences. In fact, there is one additional prolate ($\beta = 0.32$) isomeric state in ^{116}Cd. However, the energy trap around it is too shallow (the depth of the energy barrier is less than 0.04 MeV). This means the state will be delicate and collapse easily, hence is omitted in our calculations. In ^{114}Cd, the prolate ground state lies in a flat valley in the PES, which implies the nucleus may be able to deform nearly freely along its axis in the vicinity of $\beta \approx 0.12$. The energy trap at the γ-soft isomeric state is deep (over 1 MeV) in ^{112}Cd and ^{114}Cd, while in ^{110}Cd it is not. The specific values of each shape isomeric state, namely, the deformation coordinates and the energies with respect to the ground state, are summarized in Table I. The energy of some isomeric states are very close to that of the ground state. For example, the second isomeric state in ^{116}Cd is 0.007 MeV with respect to its ground state, the second isomeric state in ^{114}Cd is about 0.06 MeV. The energy of the triaxial deformed isomeric state in ^{114}Cd is also small, about 0.40 MeV. In contrast, the isomeric states in ^{110}Cd are relatively higher in energy: the oblate and the γ-soft state are 2.37 MeV and 2.60 MeV, respectively.

The prolate or oblate shapes are all rotation ellipsoids; in contrast, a triaxial-deformed sphere is further squeezed perpendicular to the rotating axis. It will contribute different content to collective motions, e.g., new rotating patterns. When a nucleus is perturbed, the γ-soft deformations may lead to different responses and it is interesting to focus on its impact on the monopole resonance.

B. Giant monopole resonance built on the shape isomeric state

The resonances built on the shape isomers can be approximated by the small vibrations in the vicinity of corresponding isomeric states. The giant resonance, which represents the collective motion of the whole nucleus, depends closely on the neutron/proton single particle levels. In general, different deformation always means changes of the single particle levels. Therefore, the excitations caused by the coherent interactions between different particle-hole pairs or two-quasiparticle pairs, will show distinct characters as the geometry of a nucleus changes. In Fig. 3, we compare the theoretical results with the experimental measurements [2], the formers are calculated with an energy spacing of 0.2 MeV. The experimental

distributions are smoother and wider than the theoretical ones, since the equivalent smear width we used here is 2.0 MeV. In order to achieve a better coincidence between theoretical and experimental results, a larger smear width seems to be necessary [31]. It is easy to see that the whole structure of the monopole resonance shifts to lower energy as the nucleus mass increases. An overall feature in all the isotopes is that the distribution of GMR strength becomes more fragmented when the deformation is larger, especially for the γ-soft deformed states. We notice that in some well-deformed nuclei, a low energy monopole mode appears as a result of the coupling between GMR and the $K = 0$ component of giant quadrupole resonance (GQR) [43–46]. However, the two-peak structure does not clearly manifest in the experimental data of Cd isotopes, or in our calculations, although the distributions of GMR are indeed broadened.

The peak position of a resonance structure can be measured quantitatively via the centroid energy, which is defined as $E_{cen} \equiv m_1/m_0$. The ith energy weighted moment can be calculated through the distribution of the strength function,

$$m_i = \int \frac{dB}{d\omega} \omega^i d\omega. \qquad (31)$$

In our calculations, the integrals are carried out over the energy region 5–40 MeV. The values of the centroid energies are listed in Table II. The theoretical predictions, i.e., the centroid energies of the GMRs built on the ground states, are more systematically overestimated than the experimental measurements are (about 0.8 MeV). The overestimations seem to be inevitable and are also reproduced by different DFT models [2], such as FSUGold [47] and NL3 [48]. Indeed, it has confused the nuclear theorist for a long time: why the well calibrated DFT models fail in predicting the right positions of the GMRs in Cd isotopes? Considering the triumphs that the DFT models have achieved in the applications both in

TABLE II. Centroid energies (in MeV) of the GMRs built on various isomeric states in the Cd isotopes. The second column contains the experimental results.

Nucl.	expt.	g.s.	2nd	3rd
^{110}Cd	15.94 ± 0.07	16.85	16.43	15.68
^{112}Cd	15.80 ± 0.05	16.54	16.36	15.52
^{114}Cd	15.61 ± 0.08	16.46	16.23	15.53
^{116}Cd	15.44 ± 0.06	16.20	15.96	15.18

nuclear matter and in a variety of finite nuclei, it is worthy to look for some nuclear structure effect to soften the GMRs in Cd isotopes.

From the data, it is interesting to notice that, in each isotope the GMR built on the higher isomeric state is always of smaller centroid energy. The centroids corresponding to the ground states in different Cd isotopes lie almost around a line. The same pattern also holds both in the oblate case and in the γ-soft case. In Fig. 4 we draw these lines with different colors and styles, which are generated via linear least square fits. The red solid line represents the result corresponding to the ground states, most of which are prolate deformed. Meanwhile, the green dotted line and the blue dashed line represent the results relating to oblate and triaxial deformations. Comparing with the experimental values, the systematical overestimations can be confirmed in the oblate case (about 0.5 MeV), while underestimations can be found in the γ-soft case (within 0.2 MeV). The results show that deformation is a mechanism to draw the resonance structure towards lower energy. Therefore, if the shape isomer mixing occurs when a cadmium isotope is vibrated, the strength function will consist of the contributions from every isomeric state, namely,

$$\frac{d\bar{B}(\hat{f}, \omega)}{d\omega} = \sum_{\theta} C_{\theta}^2 \sum_{\nu} |\langle \nu; \theta | \hat{f} | 0; \theta \rangle|^2 \delta(\omega - \omega_{\nu}^{\theta}). \quad (32)$$

$|\nu; \theta\rangle$ represents a state that is excited by the perturbation field $\hat{f}$ from a shape isomer $|0; \theta\rangle$, the energy of the excited state is ω_{ν}^{θ}. The isomer branching ratio C_{θ} is the probability that a nucleus is at its isomeric state θ, where θ denotes each possible deformation (spherical, prolate, oblate, or γ-soft). The branching ratio depends on many factors, e.g., the energy
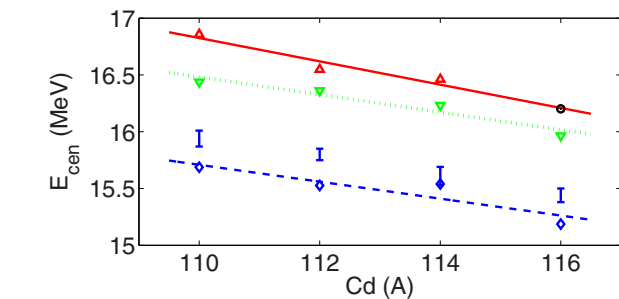

FIG. 4. The GMR centroid energies of the Cd isotopes with different deformations, compared with the experimental measurements. The value corresponding to spherical, prolate, oblate, and γ-soft state is depicted with black $\circ$, red $\triangle$, green $\triangledown$, and blue $\diamond$, respectively. Experimental results are denoted by the error bars.

of the shape isomer as well as the energy trap around it. Since the underestimation in the γ-soft case is smaller than the overestimations in the ground state case and oblate deformed case, its branching ratio must be very large, in order to reduce the centroid energies sufficiently. We hope the large branching ratio of the γ-soft isomeric state will be identified in future measurements.

When a cadmium isotope is perturbed by an external monopole field (like being bombarded by α particle beams [2]), the shape isomeric states will be easily produced due to their low energies. Usually, the lifetime of a shape isomer is very long, e.g., the shape isomer of ^{68}Ni has a lifetime about hundreds of nanoseconds [14,49]. Therefore, once the shape isomeric states are produced, the nuclei will maintain the deformed shapes until being scattered by consecutive incident particles. Isomers with prolate, oblate, and γ-soft deformations respond to the external perturbations differently, and the contribution of each kind of isomeric state to the whole strength distribution depends on its branching ratio. If the branching ratios of the γ-soft isomeric states are prominent, the giant monopole resonance will be drawn towards low energy. Therefore, a better agreement between the theoretical predictions and the experimental measurements is likely to be achieved.

IV. CONCLUSIONS

In this work we investigated the isoscalar giant monopole resonances in the even-even Cd isotopes. The linear response equation of the nucleus is solved using the finite amplitude method. Generally, the centroid energies decrease with the mass number A. The larger deformation makes the strength function of the giant monopole resonance more fragmented. The deformation plays an important role in determining how the nucleus respond to external monopole perturbations. The monopole resonances built on the isomeric states show distinct patterns, which are closely related to their deformations. There is a clear tendency that the triaxial deformation will make the centroid of the GMR lower. The shape isomer mixing, which means some γ-soft isomeric states contribute to the GMR strength when a nucleus is excited, may be helpful to explain why the centroid energies of the breathing mode in cadmium isotopes are so low.

APPENDIX: MATRIX ELEMENTS OF THE MONOPOLE OPERATOR IN THE TRIAXIAL-DEFORMED BASIS

In the triaxial deformed case, the wave functions of the single nucleon states are expanded with a three-dimensional harmonic oscillator basis,

$$\Phi_{\alpha}(\boldsymbol{r}; m_s) = \phi_{n_x}(x)\phi_{n_y}(y)\phi_{n_z}(z)\chi_{m_s}. \quad (A1)$$

In each direction ($\mu \equiv x, y, z$) involves a Hermite polynomial,

$$\phi_{n_\mu}(\mu) = (\sqrt{\pi}2^n n! b_\mu)^{-1/2} H_{n_\mu}(\zeta_\mu) e^{-\zeta_\mu^2/2}, \quad \text{(A2)}$$

where the corresponding oscillator length b_μ and the scaled dimensionless variable ζ_μ are

$$b_\mu = \sqrt{\hbar/m\omega_\mu}, \quad \zeta_\mu = \mu/b_\mu. \quad \text{(A3)}$$

The spin factor is chosen to make the triaxial harmonic oscillator basis to be an eigenfunction of the x-simplicity operator $\hat{S}_x = \hat{P}e^{-i\pi J_x}$ [34]. The positive and negative eigenvalue states are related by the time-reversal operator:

$$|n_x n_y n_z; +\rangle = |n_x n_y n_z\rangle \frac{i^{n_y}}{\sqrt{2}}[|\uparrow\rangle - (-1)^{n_x}|\downarrow\rangle],$$

$$|n_x n_y n_z; -\rangle = \hat{\mathcal{T}}|n_x n_y n_z; +\rangle. \quad \text{(A4)}$$

The matrix element of the giant monopole operator r^2 between two three-dimensional oscillator eigenfunctions can be calculated as

$$\langle n'_x n'_y n'_z | r^2 | n_x n_y n_z \rangle = \langle n'_x n'_y n'_z | x^2 + y^2 + z^2 | n_x n_y n_z \rangle$$
$$= \delta_{n'_x,n_x}\delta_{n'_y,n_y}\langle n'_z|z^2|n_z\rangle + \delta_{n'_y,n_y}\delta_{n'_z,n_z}\langle n'_x|x^2|n_x\rangle$$
$$+ \delta_{n'_z,n_z}\delta_{n'_x,n_x}\langle n'_y|y^2|n_y\rangle. \quad \text{(A5)}$$

By noticing the following integral property of two Hermite polynomials:

$$\frac{1}{\sqrt{\pi}}\int_{-\infty}^{\infty} H_m(z)H_n(z)z^2 e^{-z^2}dz$$
$$= \left(2^n m!\delta_{m,n+2} + 2^m n!\delta_{m,n-2} + 2^n n!\frac{2n+1}{2}\delta_{m,n}\right). \quad \text{(A6)}$$

The matrix element in each direction ($\mu = x, y, z$) can be easily carried out

$$\langle n'_\mu | \mu^2 | n_\mu \rangle = b_\mu^2 \left(\frac{1}{2}\sqrt{n'_\mu(n'_\mu - 1)}\delta_{n'_\mu,n_\mu+2}\right.$$
$$\left. + \frac{1}{2}\sqrt{n_\mu(n_\mu - 1)}\delta_{n'_\mu,n_\mu-2} + \frac{2n_\mu+1}{2}\delta_{n'_\mu,n_\mu}\right). \quad \text{(A7)}$$

In addition, the spin parts of the wave functions (A4) will contribute a factor $(-1)^{(n_y-n'_y)/2}$. The Bogoliubov transformation of the operator $f = r^2$ leads to

$$F_{\mu\nu}^{20} = (U^\dagger f V^* - V^\dagger f U^*)_{\mu\nu},$$
$$F_{\mu\nu}^{02} = (U^T f V - V^T f U)_{\mu\nu}. \quad \text{(A8)}$$

[1] J. Blaizot, Phys. Rep. **64**, 171 (1980).

[2] D. Patel, U. Garg, M. Fujiwara, H. Akimune, G. Berg, M. Harakeh, M. Itoh, T. Kawabata, K. Kawase, B. Nayak, T. Ohta, H. Ouchi, J. Piekarewicz, M. Uchida, H. Yoshida, and M. Yosoi, Phys. Lett. B **718**, 447 (2012).

[3] M. Bender, P.-H. Heenen, and P.-G. Reinhard, Rev. Mod. Phys. **75**, 121 (2003).

[4] T. Nakatsukasa, K. Matsuyanagi, M. Matsuo, and K. Yabana, Rev. Mod. Phys. **88**, 045004 (2016).

[5] U. Garg, T. Li, S. Okumura, H. Akimune, M. Fujiwara, M. Harakeh, H. Hashimoto, M. Itoh, Y. Iwao, T. Kawabata, K. Kawase, Y. Liu, R. Marks, T. Murakami, K. Nakanishi, B. Nayak, P. M. Rao, H. Sakaguchi, Y. Terashima, M. Uchida, Y. Yasuda, M. Yosoi, and J. Zenihiro, Nucl. Phys. A **788**, 36 (2007).

[6] J. Piekarewicz, Phys. Rev. C **76**, 031301(R) (2007).

[7] T. Li, U. Garg, Y. Liu, R. Marks, B. K. Nayak, P. V. Rao Madhusudhana, M. Fujiwara, H. Hashimoto, K. Kawase, K. Nakanishi, S. Okumura, M. Yosoi, M. Itoh, M. Ichikawa, R. Matsuo, T. Terazono, M. Uchida, T. Kawabata, H. Akimune, Y. Iwao, T. Murakami, H. Sakaguchi, S. Terashima, Y. Yasuda, J. Zenihiro, and M. N. Harakeh, Phys. Rev. Lett. **99**, 162503 (2007).

[8] L.-G. Cao, H. Sagawa, and G. Colò, Phys. Rev. C **86**, 054313 (2012).

[9] X.-W. Sun, J. Chen, and D.-H. Lu, Chin. Phys. C **42**, 14101 (2018).

[10] K. Yoshida and T. Nakatsukasa, Phys. Rev. C **88**, 034309 (2013).

[11] T. Nikšić, N. Kralj, T. Tutiš, D. Vretenar, and P. Ring, Phys. Rev. C **88**, 044327 (2013).

[12] P. Walker and G. Dracoulis, Nature **399**, 35 (1999).

[13] B. Olaizola, L. M. Fraile, H. Mach, A. Poves, F. Nowacki, A. Aprahamian, J. A. Briz, J. Cal-González, D. Ghiţa, U. Köster, W. Kurcewicz, S. R. Lesher, D. Pauwels, E. Picado, D. Radulov, G. S. Simpson, and J. M. Udías, Phys. Rev. C **95**, 061303(R) (2017).

[14] F. Recchia, D. Weisshaar, A. Gade, J. A. Tostevin, R. V. F. Janssens, M. Albers, V. M. Bader, T. Baugher, D. Bazin, J. S. Berryman, B. A. Brown, C. M. Campbell, M. P. Carpenter, J. Chen, C. J. Chiara, H. L. Crawford, C. R. Hoffman, F. G. Kondev, A. Korichi, C. Langer, T. Lauritsen, S. N. Liddick, E. Lunderberg, S. Noji, C. Prokop, S. R. Stroberg, S. Suchyta, K. Wimmer, and S. Zhu, Phys. Rev. C **94**, 054324 (2016).

[15] S. Leoni, B. Fornal, N. Mărginean, M. Sferrazza, Y. Tsunoda, T. Otsuka, G. Bocchi, F. C. L. Crespi, A. Bracco, S. Aydin, M. Boromiza, D. Bucurescu, N. Cieplicka-Oryńczak, C. Costache, S. Călinescu, N. Florea, D. G. Ghiţă, T. Glodariu, A. Ionescu, L. Iskra, M. Krzysiek, R. Mărginean, C. Mihai, R. E. Mihai, A. Mitu, A. Negreţ, C. R. Niţă, A. Olăcel, A. Oprea, S. Pascu, P. Petkov, C. Petrone, G. Porzio, A. Şerban, C. Sotty, L. Stan, I. Ştiru, L. Stroe, R. Şuvăilă, S. Toma, A. Turturică, S. Ujeniuc, and C. A. Ur, Phys. Rev. Lett. **118**, 162502 (2017).

[16] M. Girod, J. P. Delaroche, D. Gogny, and J. F. Berger, Phys. Rev. Lett. **62**, 2452 (1989).

[17] B. Crider, C. Prokop, S. Liddick, M. Al-Shudifat, A. Ayangeakaa, M. Carpenter, J. Carroll, J. Chen, C. Chiara, H. David, A. Dombos, S. Go, R. Grzywacz, J. Harker, R. Janssens, N. Larson, T. Lauritsen, R. Lewis, S. Quinn, F. Recchia, A. Spyrou, S. Suchyta, W. Walters, and S. Zhu, Phys. Lett. B **763**, 108 (2016).

[18] S. Cruz, P. Bender, R. Krücken, K. Wimmer, F. Ames, C. Andreoiu, R. Austin, C. Bancroft, R. Braid, T. Bruhn, W. Catford, A. Cheeseman, A. Chester, D. Cross, C. Diget, T. Drake, A. Garnsworthy, G. Hackman, R. Kanungo, A. Knapton, W. Korten, K. Kuhn, J. Lassen, R. Laxdal, M. Marchetto, A. Matta, D. Miller, M. Moukaddam, N. Orr, N. Sachmpazidi, A. Sanetullaev, C. Svensson, N. Terpstra, C. Unsworth, and P. Voss, Phys. Lett. B **786**, 94 (2018).

[19] P. Möller, A. J. Sierk, R. Bengtsson, H. Sagawa, and T. Ichikawa, Phys. Rev. Lett. **103**, 212501 (2009).

[20] F. Recchia, C. J. Chiara, R. V. F. Janssens, D. Weisshaar, A. Gade, W. B. Walters, M. Albers, M. Alcorta, V. M. Bader, T. Baugher, D. Bazin, J. S. Berryman, P. F. Bertone, B. A. Brown, C. M. Campbell, M. P. Carpenter, J. Chen, H. L. Crawford, H. M. David, D. T. Doherty, C. R. Hoffman, F. G. Kondev, A. Korichi, C. Langer, N. Larson, T. Lauritsen, S. N. Liddick, E. Lunderberg, A. O. Macchiavelli, S. Noji, C. Prokop, A. M. Rogers, D. Seweryniak, S. R. Stroberg, S. Suchyta, S. Williams, K. Wimmer, and S. Zhu, Phys. Rev. C **88**, 041302(R) (2013).

[21] S. Suchyta, S. N. Liddick, Y. Tsunoda, T. Otsuka, M. B. Bennett, A. Chemey, M. Honma, N. Larson, C. J. Prokop, S. J. Quinn, N. Shimizu, A. Simon, A. Spyrou, V. Tripathi, Y. Utsuno, and J. M. VonMoss, Phys. Rev. C **89**, 021301(R) (2014).

[22] Y. Tsunoda, T. Otsuka, N. Shimizu, M. Honma, and Y. Utsuno, Phys. Rev. C **89**, 031301(R) (2014).

[23] X. Sun, J. Chen, and D. Lu, Phys. Rev. C **98**, 024607 (2018).

[24] P. Ring and P. Schuck, *The Nuclear Many-Body Problem* (Springer, Berlin, 2004).

[25] D. Vretenar, N. Paar, T. Marketin, and P. Ring, J. Phys. G: Nucl. Part. Phys. **35**, 014039 (2008).

[26] K. Yoshida and N. V. Giai, Phys. Rev. C **78**, 064316 (2008).

[27] Y. Niu, N. Paar, D. Vretenar, and J. Meng, Phys. Lett. B **681**, 315 (2009).

[28] X. Sun, J. Chen, and D. Lu, Phys. Rev. C **99**, 054604 (2019).

[29] T. Nakatsukasa, T. Inakura, and K. Yabana, Phys. Rev. C **76**, 024318 (2007).

[30] M. Kortelainen, N. Hinohara, and W. Nazarewicz, Phys. Rev. C **92**, 051302(R) (2015).

[31] X. Sun and D. Lu, Phys. Rev. C **96**, 024614 (2017).

[32] K. Washiyama and T. Nakatsukasa, Phys. Rev. C **96**, 041304(R) (2017).

[33] J. G. Valatin, Phys. Rev. **122**, 1012 (1961).

[34] T. Nikšić, N. Paar, D. Vretenar, and P. Ring, Comput. Phys. Commun. **185**, 1808 (2014).

[35] G. A. Lalazissis, T. Nikšić, D. Vretenar, and P. Ring, Phys. Rev. C **71**, 024312 (2005).

[36] P. G. Reinhard, Rep. Prog. Phys. **52**, 439 (1989).

[37] Y. Tian, Z. Ma, and P. Ring, Phys. Lett. B **676**, 44 (2009).

[38] D. Pena Arteaga and P. Ring, Phys. Rev. C **77**, 034317 (2008).

[39] P. Avogadro and T. Nakatsukasa, Phys. Rev. C **87**, 014331 (2013).

[40] D. D. Johnson, Phys. Rev. B **38**, 12807 (1988).

[41] B. R. Mottelson and A. N. Bohr, *Nuclear Structure* (World Scientific, Singapore, 1998), Vol. 2.

[42] D. L. Hill and J. A. Wheeler, Phys. Rev. **89**, 1102 (1953).

[43] J. Kvasil, V. O. Nesterenko, A. Repko, D. Bozik, W. Kleinig, and P.-G. Reinhard, J. Phys. Conf. Ser. **580**, 012053 (2015).

[44] Y. K. Gupta, U. Garg, J. Hoffman, J. Matta, P. V. Madhusudhana Rao, D. Patel, T. Peach, K. Yoshida, M. Itoh, M. Fujiwara, K. Hara, H. Hashimoto, K. Nakanishi, M. Yosoi, H. Sakaguchi, S. Terashima, S. Kishi, T. Murakami, M. Uchida, Y. Yasuda, H. Akimune, T. Kawabata, and M. N. Harakeh, Phys. Rev. C **93**, 044324 (2016).

[45] K. Yoshida, Phys. Rev. C **82**, 034324 (2010).

[46] J. Kvasil, V. O. Nesterenko, A. Repko, W. Kleinig, and P.-G. Reinhard, Phys. Rev. C **94**, 064302 (2016).

[47] B. G. Todd-Rutel and J. Piekarewicz, Phys. Rev. Lett. **95**, 122501 (2005).

[48] G. A. Lalazissis, J. König, and P. Ring, Phys. Rev. C **55**, 540 (1997).

[49] O. Sorlin, S. Leenhardt, C. Donzaud, J. Duprat, F. Azaiez, F. Nowacki, H. Grawe, Z. Dombrádi, F. Amorini, A. Astier, D. Baiborodin, M. Belleguic, C. Borcea, C. Bourgeois, D. M. Cullen, Z. Dlouhy, E. Dragulescu, M. Górska, S. Grévy, D. Guillemaud-Mueller, G. Hagemann, B. Herskind, J. Kiener, R. Lemmon, M. Lewitowicz, S. M. Lukyanov, P. Mayet, F. de Oliveira Santos, D. Pantalica, Y.-E. Penionzhkevich, F. Pougheon, A. Poves, N. Redon, M. G. Saint-Laurent, J. A. Scarpaci, G. Sletten, M. Stanoiu, O. Tarasov, and C. Theisen, Phys. Rev. Lett. **88**, 092501 (2002).